

THE BLUE HOOK POPULATIONS OF MASSIVE GLOBULAR CLUSTERS¹

THOMAS M. BROWN², ALLEN V. SWEIGART³, THIERRY LANZ⁴, ED SMITH², WAYNE B. LANDSMAN⁵, IVAN HUBENY⁶

To appear in The Astrophysical Journal

ABSTRACT

We present new *HST* ultraviolet color-magnitude diagrams of 5 massive Galactic globular clusters: NGC 2419, NGC 6273, NGC 6715, NGC 6388, and NGC 6441. These observations were obtained to investigate the “blue hook” phenomenon previously observed in UV images of the globular clusters ω Cen and NGC 2808. Blue hook stars are a class of hot (approximately 35,000 K) subluminous horizontal branch stars that occupy a region of the HR diagram that is unexplained by canonical stellar evolution theory. By coupling new stellar evolution models to appropriate non-LTE synthetic spectra, we investigate various theoretical explanations for these stars. Specifically, we compare our photometry to canonical models at standard cluster abundances, canonical models with enhanced helium (consistent with cluster self-enrichment at early times), and flash-mixed models formed via a late helium-core flash on the white dwarf cooling curve. We find that flash-mixed models are required to explain the faint luminosity of the blue hook stars, although neither the canonical models nor the flash-mixed models can explain the range of color observed in such stars, especially those in the most metal-rich clusters. Aside from the variation in the color range, no clear trends emerge in the morphology of the blue hook population with respect to metallicity.

Subject headings: globular clusters: general – globular clusters: individual (NGC 2419, NGC 6273, NGC 6715, NGC 2808, NGC 6388, NGC 6441) – stars: atmospheres – stars: evolution – stars: horizontal branch – ultraviolet: stars

1. INTRODUCTION

Understanding the formation history and chemical evolution of the Galactic globular clusters has always been a formidable, but fundamental, task. However, this task has become even more challenging with the recent discovery of complex stellar populations within individual globular clusters. The most well-known example is ω Cen (Anderson 1997; Bedin et al. 2004; Ferraro et al. 2004), but the same phenomenon has also been discovered in other massive globular clusters, including NGC 2808 (D’Antona et al. 2005; Piotto et al. 2007), NGC 1851 (Milone et al. 2008; Han et al. 2009), NGC 6715 (M54; Layden & Sarajedini 2000; Siegel et al. 2007), and NGC 104 (47 Tuc; Anderson et al. 2009). In ω Cen, accurate photometry demonstrates that its main sequence (MS) population is split into multiple sequences, with the bluest MS stars being more metal rich, implying that the corresponding sub-population is perhaps enhanced in helium ($Y \sim 0.4$; Piotto et al. 2005). Such helium-rich stars may have formed in a second stellar generation from the helium-rich ejecta of the initial stellar generation that formed the cluster (e.g., see Renzini 2008). Possible candidates for producing these ejecta include asymptotic-giant-branch (AGB) stars, massive MS stars, type II supernovae, and even stars external to the cluster (Bekki & Norris 2006 and references therein). These clusters thus refute the long-standing premise that glob-

ular clusters are simple stellar populations.

The discovery of complex populations in globular clusters has understandably generated much excitement, especially in regard to the morphology of the horizontal branch (HB). Because the MS turnoff (MSTO) mass decreases strongly with increasing helium at a fixed cluster age, a high helium abundance will lead to a bluer HB morphology for a given range in the red-giant branch (RGB) mass loss, and this, in turn, might account for the long blue HB tails found in some clusters (D’Antona et al. 2002; Busso et al. 2007). In this scenario, the extreme HB (EHB) stars, located at the hot end of the HB at temperatures $T_{\text{eff}} \gtrsim 16,000$ K and surface gravities $\log g > 5$, would be the progeny of the most helium-rich MS stars. The hottest EHB stars have extremely thin envelope masses ($\sim 10^{-3} M_{\odot}$), due to extensive mass loss on the RGB. The analogs of the EHB stars in the field are the subdwarf B (sdB) stars. Both unresolved spectroscopy and resolved imaging have demonstrated that EHB stars are the dominant contributors to the “UV upturn” in the otherwise cool spectra of elliptical galaxies (Brown et al. 1997; Brown et al. 2000; Brown et al. 2008).

UV observations of globular clusters have revealed yet another puzzling result, namely, that two of the massive clusters with evidence for a helium-rich MS population (ω Cen and NGC 2808) also contain an unexpected population of subluminous EHB stars that cannot be explained by canonical stellar evolution theory. These subluminous stars were first discovered in ω Cen (D’Cruz et al. 1996, 2000), where they form a “blue hook” (BH) feature at the hot end of the canonical EHB. D’Cruz et al. (1996) proposed that such stars may have undergone a delayed helium-core flash after peeling away from the RGB due to high mass loss.

We now know that stars can follow a variety of evolutionary paths to the HB, depending on when the helium-core flash occurs (see Figure 1). For normal rates of mass loss, the helium-core flash will occur at the tip of the RGB (RGB tip flasher,

¹ Based on observations made with the NASA/ESA Hubble Space Telescope, obtained at STScI, and associated with proposal 10815.

² Space Telescope Science Institute, 3700 San Martin Drive, Baltimore, MD 21218; tbrown@stsci.edu, edsmith@stsci.edu

³ Code 667, NASA Goddard Space Flight Center, Greenbelt, MD 20771; allen.v.sweigart@nasa.gov

⁴ Department of Astronomy, University of Maryland, College Park, MD 20742; lanz@astro.umd.edu

⁵ Adnet Systems, NASA Goddard Space Flight Center, Greenbelt, MD 20771; wayne.b.landsman@nasa.gov

⁶ Steward Observatory, University of Arizona, Tucson, AZ 85712; hubeny@aegis.as.arizona.edu

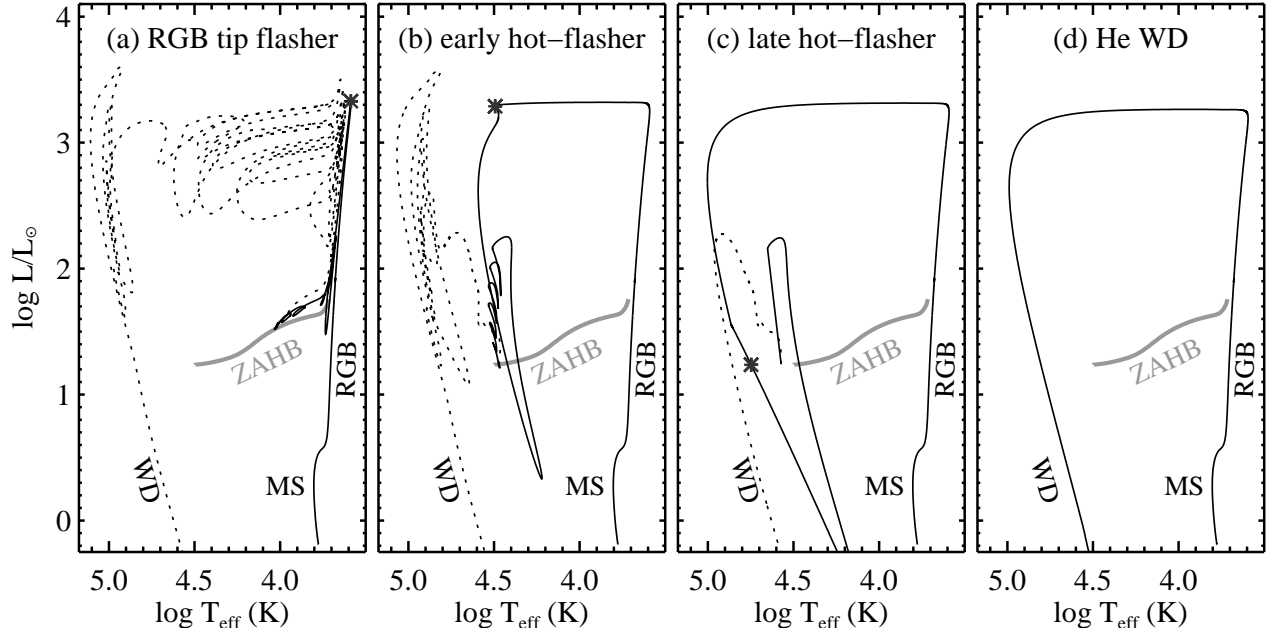


Figure 1. Various evolutionary paths for producing an HB star. The zero-age HB (ZAHB) phase is highlighted in grey, while the pre-ZAHB evolution (*solid curves*) and post-ZAHB evolution (*dashed curves*) are in black. The peak of the helium-core flash is marked by an asterisk. The four panels show the evolution for progressively larger amounts of mass loss on the RGB. The evolution in the first two panels produces canonical HB stars in which the H-rich surface composition does not change during the helium-core flash. In the third panel, the helium-core flash occurs on the WD cooling curve, producing a flash-mixed star having a surface composition highly enriched in helium and carbon and a temperature significantly hotter than the canonical HB. In the fourth panel, the helium flash never occurs and the star dies as a helium WD.

Figure 1a). However, for sufficiently high rates of mass loss, the helium-core flash can occur either during the crossing of the HR diagram (early hot flasher, Figure 1b) or on the white dwarf (WD) cooling curve (late hot flasher, Figure 1c), as first shown by Castellani & Castellani (1993). Brown et al. (2001; hereafter Paper I) demonstrated that a delayed helium-core flash on the WD cooling curve would result in a stellar atmosphere extremely enhanced in helium ($\sim 96\%$ by mass) and carbon ($\sim 4\%$ by mass), due to the mixing of the stellar envelope into the hot helium-burning core. This “flash mixing” decreases the opacity below the Lyman limit, thereby lowering the flux at longer wavelengths, and increases the effective temperature in the EHB stars. In Paper I, we found that both of these effects together might explain the BH feature in the color-magnitude diagram (CMD) of NGC 2808. Evidence for BH populations in other clusters soon followed, including NGC 6715 (Rosenberg et al. 2004), NGC 6388 (Busso et al. 2007), NGC 2419 (Ripepi et al. 2007), and NGC 6273 (noted by Rosenberg et al. 2004, but originally appearing in Piotto et al. 1999). NGC 6441 may host BH stars, although the case has been unclear (Busso et al. 2007; Dieball et al. 2009).

To extend the investigations enabled by UV observations of ω Cen and NGC 2808, we have obtained far-UV and near-UV images of those additional clusters with the strongest evidence for BH populations: NGC 2419, NGC 6273 (M19), NGC 6715 (M54), NGC 6388, and NGC 6441. A characterization of BH populations in globular clusters can only be performed definitively with an ultraviolet CMD, where, due to the small bolometric correction, the photometric effects of enhanced helium and carbon abundances can be distinguished from changes in temperature. These clusters span a wide range of metallicity ($-2.1 \leq [\text{Fe}/\text{H}] \leq -0.5$), which enables an exploration of how the BH population is distributed in temperature, luminosity, and size, relative to the canonical EHB population, as a function of cluster environment and metallic-

ity.

To avoid confusion, it is worth clarifying our terminology. BH stars were first defined observationally as being hotter and fainter than the hot end of the canonical EHB. However, we will show in this paper that some clusters host stars fainter than the canonical EHB, but with somewhat redder colors. These red colors may imply temperatures down to $\sim 15,000\text{K}$. The stars appear distinct from the still redder blue straggler sequence (BSS), and they appear to be associated with the bluer BH stars. We will also consider these to be BH stars, without necessarily implying that they have the same physical origin.

In this paper, we compare our UV CMDs of five massive globular clusters, together with the previous UV CMD of NGC 2808, to the expectations from canonical evolution theory and flash-mixing. In each case, we explore the expectations for stars born at standard cluster abundances and for stars born with enhanced helium abundances. To ensure a consistent exploration of these scenarios, our evolutionary models are tailored to the appropriate abundance profiles, as are the model atmospheres and synthetic spectra employed to transform from the theoretical plane to the observable plane.

2. OBSERVATIONS AND DATA REDUCTION

The six clusters discussed herein have all been imaged in the far-UV and near-UV using the *Hubble Space Telescope* (*HST*). Due to variations in the instrumentation available for each observation, the bandpasses were not identical for each cluster (see Figure 2), but the effective wavelengths in each wavelength region (far-UV or near-UV) are similar, easing comparison of CMDs constructed from these bandpasses. In Table 1, we summarize the observations for each cluster. We also include NGC 2808, the subject of Paper I, observed with the Space Telescope Imaging Spectrograph (STIS); each STIS UV channel has pixels of 0.025×0.025 arcsec and a field of view of 25×25 arcsec.

Table 1
Ultraviolet Imaging

Cluster	far-UV		near-UV	
	bandpass	exposure (s)	bandpass	exposure (s)
NGC2419	ACS/SBC/F150LP	5180	ACS/HRC/F250W	5080
NGC6273	ACS/SBC/F150LP	1980	WFPC2/WF3/F255W	11000
NGC6715	ACS/SBC/F150LP	1980	WFPC2/WF3/F255W	11000
NGC2808	STIS/FUV/F25Q TZ	8916	STIS/NUV/F25CN270	8906
NGC6388	ACS/SBC/F150LP	1980	WFPC2/WF3/F255W	11000
NGC6441	ACS/SBC/F150LP	4680	WFPC2/WF3/F255W	11000

As originally proposed, the observations in the current program intended to use the Solar Blind Channel (SBC) and High Resolution Channel (HRC) of the Advanced Camera for Surveys (ACS) on *HST*, with the SBC F150LP filter providing the far-UV bandpass and the HRC F250W filter providing the near-UV bandpass. The ACS/SBC has pixels of 0.034×0.030 arcsec and a field of view (FOV) of 34.6×30.1 arcsec, while the ACS/HRC has pixels of 0.028×0.025 arcsec and a FOV of 29×26 arcsec. Due to its larger distance and smaller angular size, the observations of NGC 2419 were planned with a single tile imaged with the SBC and HRC, while the remaining four clusters were planned with a 2×2 mosaic of tiles in each bandpass. Due to guide star problems and instrument failures, the program did not proceed according to plan.

In December 2006, the first observations of NGC 2419 were attempted. The HRC exposures were obtained in two consecutive orbits, with no problems. The SBC exposures were obtained in the subsequent two orbits, but with serious problems. The guide star re-acquisition failed in the first SBC orbit, setting the Take Data Flag down and resulting in two blank images. In the final orbit, the re-acquisition of guide stars was successful, but due to a flight software bug, the telescope did not complete the maneuvers needed to point at the correct field. As a consequence, the next two exposures were not blank but offset by nearly an arcmin from the successful HRC images. This flight software bug, which was apparently unique to the *HST* two-gyro mode in the situation where successful guide star acquisitions followed guide star failures in the same visit, has since been fixed. The SBC exposures for NGC 2419 were eventually obtained a year later. In short, NGC 2419 was observed with the intended ACS/SBC/F150LP and ACS/HRC/F250W bandpasses, after some difficulties.

Due to a failure of an ACS power supply in January 2007, the HRC channel stopped working. At that time, only the near-UV (HRC) images of NGC 2419 had been taken, so the near-UV images of the remaining four clusters were obtained with the Wide Field and Planetary Camera 2 (WFPC2), using the F255W filter and the WF3 chip. The WF3 chip has 0.1×0.1 arcsec pixels and a FOV of 80×80 arcsec. The near-UV channel on WFPC2 is not as sensitive as that on the ACS/HRC, but the larger field of view allowed imaging of the intended area in a single pointing instead of the 2×2 mosaic of HRC images. Thus, NGC 6273, NGC 6388, NGC 6441, and NGC 6715 were observed with the ACS/SBC/F150LP and WFPC2/F255W bandpasses.

Due to these distinctions, the observations of NGC 2419 and the remaining four clusters were processed somewhat differently. For NGC 2419, the images in each channel were registered and drizzled to a common scale of $0.''025$, while for the other four clusters, the scale was $0.''0455$. The ACS/SBC images were combined using the drizzle package (Fruchter & Hook 2002), but required no cosmic-ray rejection because

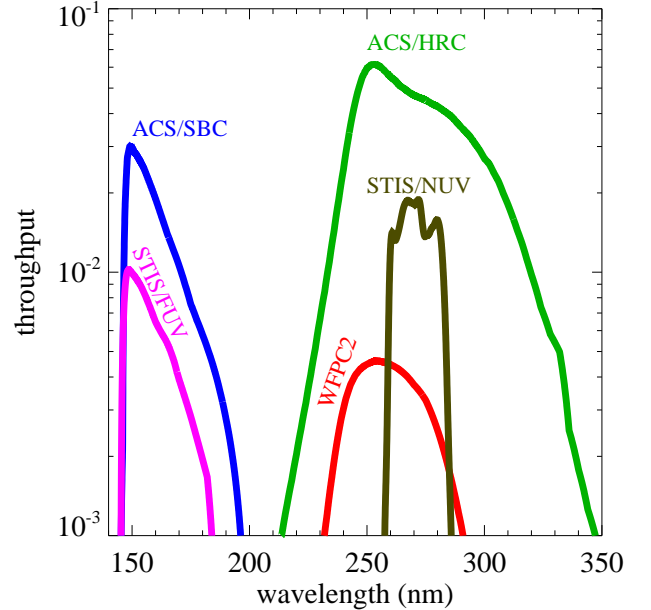


Figure 2. The bandpasses employed in our UV imaging (see Table 1).

the SBC is a photon-counting multianode microchannel array (MAMA). The WFPC2 and ACS/HRC detectors are CCDs, so images from these detectors were combined with masking of cosmic rays.

Because globular clusters are much sparser in the UV than in the optical, we did not perform photometry using fitting of the point spread function. Instead, we performed aperture photometry in each channel with an aperture correction to an infinite aperture, using the standard aperture corrections for these instruments (Heyer et al. 2004; Maybhate et al. 2010; Sirianni et al. 2005). For the four clusters observed with the ACS/SBC and WFPC2, the apertures were 2.5 pixels and 5 pixels, respectively; for the cluster observed with the ACS/SBC and ACS/HRC (NGC 2419), the apertures were 2.5 pixels and 1.5 pixels, respectively. Because it is a MAMA, the SBC requires no correction for charge transfer inefficiency (CTI), but the near-UV photometry was corrected for CTI using the corrections of Dolphin (2000) and Chiaberge et al. (2009), for the WFPC2 and ACS/HRC, respectively.

The CMD for each cluster is shown in Figure 3. In Figure 4, we highlight one of these clusters (NGC 6715) to provide a guide to the various classes of stars discussed in this paper: blue HB (BHB) stars, EHB stars, BH stars, BSS, and the AGB-Manqué (AGBM) progeny of the EHB stars. Note that we chose NGC 6715 not because it is particularly representative of massive clusters but because each class of star is well-populated in this CMD. Each cluster exhibits a distinct hook feature at the blue end of its HB locus. As discussed extensively in Paper I, this hook feature cannot be due to photo-

metric scatter, differential reddening, or instrumental effects, because these mechanisms could not affect the photometry of the EHB without also affecting the photometry of the neighboring BHB stars, which are only slightly redder; the EHB and BHB stars have similar far-UV luminosity and photometric errors. Despite the similar photometric errors in the EHB and BHB stars, the EHB locus spans a luminosity range that is several times larger than that on the hot end of the BHB.

3. MODELS

3.1. *Stellar Evolutionary Models*

The stellar evolutionary models used in the present study were computed with a procedure similar to the one described in Paper I. For each cluster, we constructed grids of evolutionary sequences that followed the evolution of appropriate low-mass stars continuously from the zero-age MS through the end of the HB phase for two values of the initial helium abundance: a helium-normal abundance Y of 0.23, representing the helium abundance in stars born during the first stellar generation with standard cluster abundances, and a helium-rich abundance Y of 0.40, representing a reasonable upper limit on the helium enhancement in the second stellar generation born after a process of cluster self-enrichment. The hotter HB sequences in these grids were also evolved through the post-HB phases.

The heavy element abundance Z for these sequences was determined from the observed $[\text{Fe}/\text{H}]$ value for each cluster, assuming an α -element enhancement of $[\alpha/\text{Fe}] = 0.3$, as appropriate for metal-poor globular cluster stars (Carney 1996). Using the prescription given by Salaris et al. (1993) for converting an α -enhanced abundance into an equivalent scaled-solar abundance, we obtained scaled-solar heavy element abundances Z of 0.00023, 0.00064, 0.00081, 0.0015, 0.0077, and 0.0090, respectively, for the six clusters NGC 2419, NGC 6273, NGC 6715, NGC 2808, NGC 6388 and NGC 6441. We used the same Z value to compute both the helium-normal and helium-rich sequences for each cluster. The initial main sequence mass for each composition (Y , Z) was calculated for an age of 13 Gyr at the tip of the RGB, although ages a few Gyr younger would have little qualitative effect on the subsequent evolutionary behavior.

The sequences for each composition (Y , Z) differ from each other only in the amount of mass loss along the RGB, which we parameterize with the Reimers (1975, 1977) mass-loss formulation:

$$\dot{M} = -4 \times 10^{-13} \eta_R L / g R \quad (M_\odot \text{ yr}^{-1}),$$

where L , g , and R are the stellar luminosity, gravity, and radius, respectively, in solar units, and η_R is the well-known Reimers mass-loss parameter. Because our calculations follow the evolution through the helium-core flash, we are able to determine how the evolutionary path from the MS to the ZAHB depends on the assumed mass-loss rate (see Figure 1). The red end of the ZAHB is set by the sequence with $\eta_R = 0.0$ (no mass loss). Up to a given value of η_R (~ 0.7 for intermediate $[\text{Fe}/\text{H}]$ values), the models remain tightly bound to the RGB until the helium-core flash (Figure 1a). However, for higher values of η_R , the models leave the RGB and evolve to high effective temperatures before igniting helium (Castellani & Castellani 1993), either during the crossing of the CMD (Figure 1b) or while descending the WD cooling curve (Figure 1c). D’Cruz et al. (1996) suggested that such “hot flashers” might provide another channel for populating the EHB. Although the masses of the late hot flashers for each com-

position (Y , Z) fall within a narrow range, they are produced over a rather wide range in the mass loss rate ($\Delta\eta_R \sim 0.1$). Extremely fine tuning of the mass-loss rate is thus not required to produce a late hot flasher (see Paper I). For sufficiently high values of η_R , the models simply cross the HR diagram and descend the WD cooling curve without igniting helium, thus dying as helium WDs (see Figure 1d).

The RGB tip flashers and early hot flashers ignite helium at a time when the models are very luminous. The strong hydrogen-burning shell in these models forms a high entropy barrier that prevents the flash convection from penetrating into the envelope, and hence no mixing then occurs between the envelope and the core. Thus any star that undergoes the helium-core flash before reaching the WD cooling curve will arrive on the ZAHB via canonical evolution (i.e., with a normal atmospheric composition). In contrast, stars that ignite helium on the WD cooling curve have much weaker hydrogen-burning shells and thus much lower entropy barriers (Sweigart 1997; Paper I). Under these conditions, penetration of the flash convection into the envelope becomes inevitable. This flash mixing will mix hydrogen-rich material from the envelope into the core and helium- and carbon-rich material from the core into the envelope, thereby greatly enhancing the surface helium and carbon abundances. A similar process may produce other extremely hydrogen-poor stars (also known as “born again” stars) during a very late helium-*shell* flash (Renzini 1990).

Due to the numerical difficulties associated with this mixing process (Paper I), we terminated our sequences as soon as they encountered flash mixing. Nevertheless, we can still predict the surface composition that these flash-mixed models should have when they arrive on the ZAHB. The available calculations clearly indicate that flash mixing will consume most, if not all, of the envelope hydrogen. Thus we expect the surface composition of the flash-mixed models to be strongly depleted in hydrogen and enriched in helium. The surface carbon abundance should also be close to its value in the flash convection zone, namely, 4% by mass. For these reasons the flash-mixed models given in this paper will assume that the surface carbon abundance has been increased to 4% by mass and that all of the remaining surface hydrogen has been burned to helium. It is worth noting that Cassisi et al. (2003) and Miller Bertolami et al. (2008) were able to follow the flash mixing process in detail, and their values for the flash-mixed surface composition are in good agreement with the composition adopted here. Note also that some of the carbon may be burned to nitrogen during the flash mixing, depending on the details of the nucleosynthesis; such an outcome would not have a significant effect on the stellar evolution models.

3.2. *Non-LTE Model Atmospheres and Synthetic Spectra*

In order to produce theoretical spectra for the evolutionary tracks, we calculated a series of 60 non-LTE line-blanketed model atmospheres with our model atmosphere program, TLUSTY, version 201⁷. For each globular cluster, we used the appropriate metallicities and helium abundances for the various evolutionary scenarios explored. TLUSTY computes stellar model photospheres in a plane-parallel geometry, assuming radiative and hydrostatic equilibria. Departures from LTE are explicitly allowed for a large set of chemical species and arbitrarily complex model atoms, using our hybrid Complete Linearization/Accelerated Lambda Iteration method (Hubeny

⁷ Available at <http://nova.astro.umd.edu>

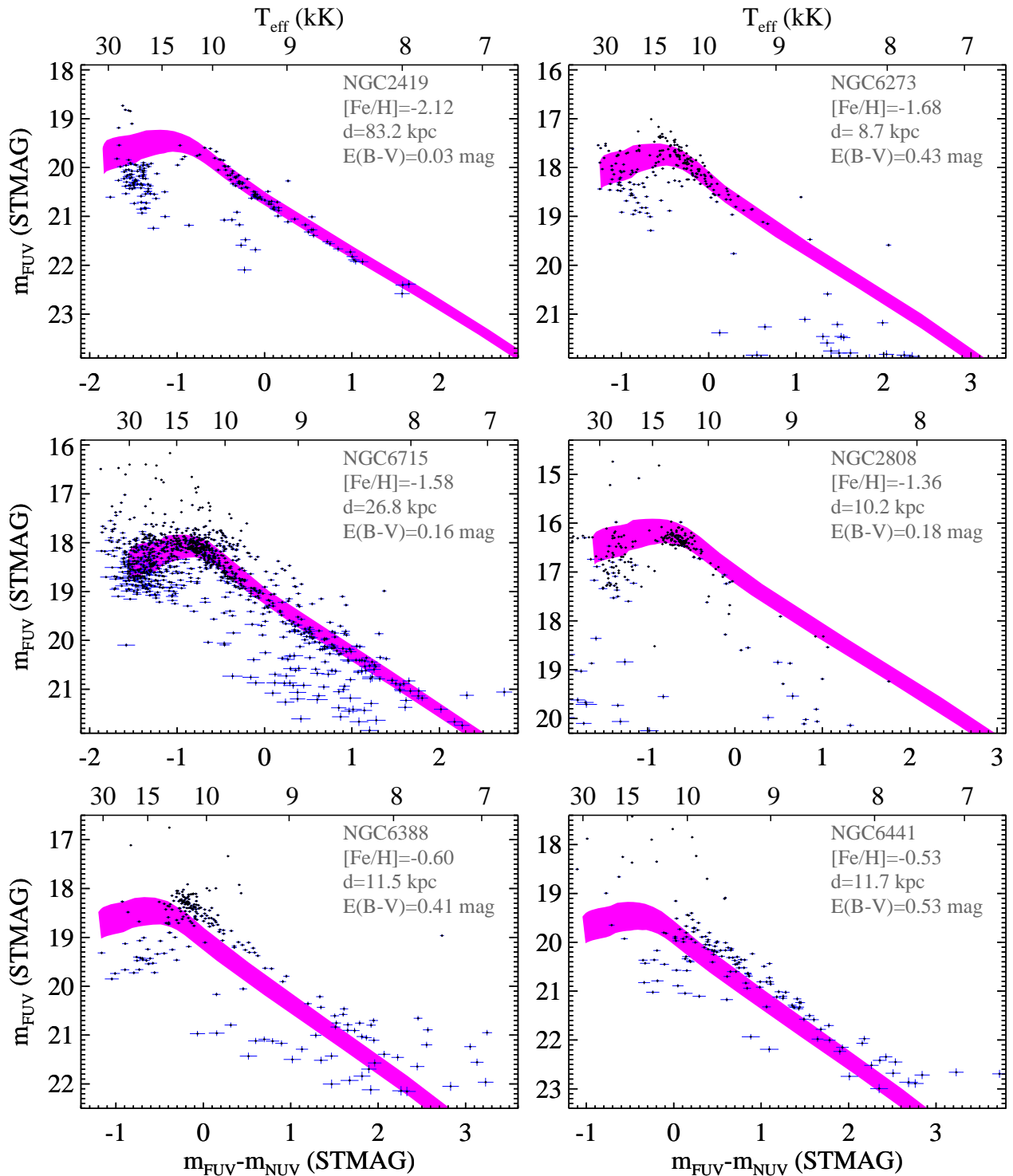


Figure 3. Ultraviolet CMDs for six massive globular clusters spanning a wide range in $[\text{Fe}/\text{H}]$ (points), along with the HB locus expected from canonical stellar evolution theory at standard helium abundance ($Y = 0.23$; violet shaded area). The assumed cluster parameters are indicated (grey labels). An approximate conversion (assuming normal cluster abundances) between observed color and effective temperature is shown on the upper abscissa in each panel. Photometric errors (blue bars) are only significant for stars much redder and fainter than the EHB stars that are the focus of this paper. The BH population appears as a downward hook at the blue end of the observed HB, where it deviates below the canonical EHB. For the two metal-rich clusters, that deviation occurs far to the red of the hot end of the canonical HB.

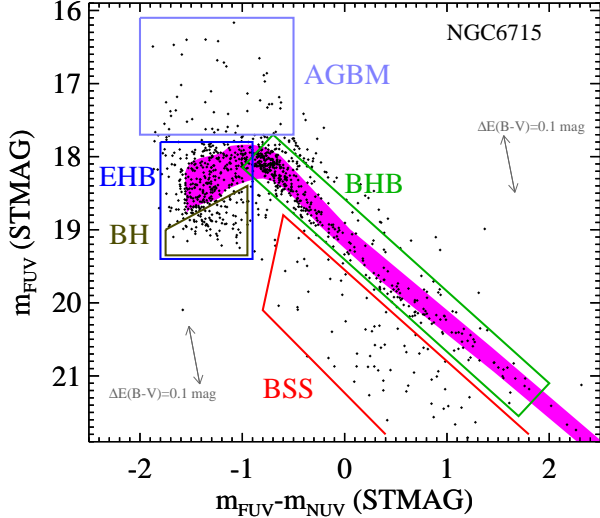


Figure 4. The ultraviolet CMD of NGC 6715 (points), along with the expected HB locus based upon canonical evolutionary models at standard helium abundance (violet shaded area). The various classes of stars are indicated (colored boxes). The BH stars are the subluminous subset of the EHB stars. Reddening vectors for both redder and bluer stars are indicated (labeled grey arrows)

& Lanz 1995). More specifically, the model atmospheres allow for departures from LTE for 1132 levels and superlevels of 52 ions, H I, He I, He II, C I – C IV, N I – N V, O I – O VI, Ne I – Ne IV, Mg II, Al II, Al III, Si II – Si IV, P IV, P V, S II – S VI, Fe II – Fe VI. Details of the model atom setup are provided in Lanz & Hubeny (2003, 2007), and in Cunha et al. (2006) for updated Neon models.

The model atmospheres span the range of parameters suitable for most EHB stars: $20,000 \text{ K} \leq T_{\text{eff}} \leq 50,000 \text{ K}$ (with a 5,000 K step), $4.5 \leq \log g \leq 6.0$ (0.5 dex step), and $V_{\text{turb}} = 5 \text{ km/s}$. We assumed three different helium compositions: standard helium ($Y = 0.23$), helium-rich ($Y = 0.4$), and flash-mixed ($Y = 0.96$, with carbon and nitrogen mass fractions of 3% and 1%, respectively; Lanz et al. 2004 – hereafter Paper II). Note that the assumption of 4% carbon or 4% nitrogen (or some intermediate mix) makes little difference in broad-band UV colors (see Paper I).

With our spectrum synthesis code, SYNSPEC, we then calculated the detailed emergent ultraviolet spectrum of each model atmosphere. Quadratic interpolations in the spectra database were performed to derive theoretical far-UV and near-UV magnitudes for the specific stellar parameters along each evolutionary track. The parameters of the quadratic interpolation are wavelength-dependent. Detailed tests show that this interpolation process yields colors that do not differ by more than 0.01 mag, compared to using a model atmosphere calculated with the exact stellar parameters. This approach saves significant computing time without significantly affecting the final accuracy.

3.3. Transfer of Models to the Color-Magnitude Diagrams

With these models in hand, we transformed the evolutionary models for each cluster to the observable plane. For each cluster, we interpolated in the grid of synthetic spectra having the appropriate abundance pattern (cluster metallicity with $Y = 0.23$, cluster metallicity with $Y = 0.4$, or the flash-mixed composition). For stars cooler than the lowest effective temperature in our non-LTE grids, we interpolated in the Castelli & Kurucz (2003) spectral grids at enhanced $[\alpha/\text{Fe}]$. The in-

terpolated spectrum for each stellar evolutionary model was reddened using the average Galactic extinction curve of Fitzpatrick (1999), and then passed through the relevant near-UV and far-UV bandpasses using the IRAF SYNPHOT package, resulting in magnitudes in the STMAG system, where $m = -2.5 \times \log_{10} f_{\lambda} - 21.1 \text{ mag}$. Note that this method appropriately applies the reddening in a bandpass-dependent and T_{eff} -dependent manner.

4. COMPARISON OF PHOTOMETRY TO MODELS

4.1. Canonical Models at Standard Helium Abundance

We first compare our CMDs to the expectations from canonical stellar evolutionary models with a standard helium abundance. We use the BHB as a standard candle to guide the normalization of these models. Specifically, we adopt metallicity and distance values that are representative of values in the literature, and then make small adjustments to the extinction so as to place the BHB of a canonical model at the expected location. Note that the reddening vector in our m_{FUV} vs. $m_{\text{FUV}} - m_{\text{NUV}}$ CMDs is nearly vertical, so one could adjust the distance instead of the reddening, or some combination thereof; a change of 0.01 mag in $E(B - V)$ is equivalent to a change of 0.079 mag in distance modulus. For the four metal-poor clusters, the theoretical HB distribution should be coincident with the observed HB locus at the BHB. For the two metal-rich clusters, Rich et al. (1997) have shown that the HB slopes strongly upward as one moves from the reddest HB stars to the BHB (see also Busso et al. 2007), such that the BHB is $\sim 0.5 \text{ mag}$ brighter in the optical than one would expect for a canonical locus normalized to the red HB. It would be simpler to consistently align our models to the red HB in all of our clusters, but it falls outside of our UV CMDs, driving our use of the BHB; thus, for the two metal-rich clusters we choose an extinction that places the canonical locus 0.5 mag fainter in the far-UV than the observed BHB locus. We are assuming that a star at a given reference point on the BHB (defined at a particular effective temperature) has changed in bolometric luminosity, such that the offset in the far-UV is the same 0.5 mag observed in the optical. The physical motivation for this assumption comes from the fact that the bolometric luminosities of all HB stars in the range $6000 \lesssim T_{\text{eff}} \lesssim 18000 \text{ K}$ are increased by nearly the same amount when Y is enhanced, and that the effect on the UV-to-optical color in the emergent spectrum is minimal. As we shall see in the next section, our choice of extinction is equivalent to aligning canonical BHB models of intermediate Y (~ 0.3) to the observed BHB locus.

In Figure 3, we show the CMD of each cluster compared to the expected locus for stars in the core helium-burning stage, assuming standard cluster metallicity and helium abundance. The comparison is made over a wide color range that includes stars much redder than the EHB. In Figure 5, we restrict the comparison to those stars hotter than $\sim 9,000 \text{ K}$, and shade the HB locus to indicate the timescales expected for HB evolution. We expect most of the HB stars to follow close to the low-luminosity edge of the canonical helium-burning locus, because the evolution accelerates towards the latter stages of the HB phase (i.e., from the bottom to the top of the canonical HB locus). Because we use the BHB as a standard candle to normalize the models, we can make an appropriate comparison of the observed EHB locus and the predicted EHB locus.

NGC 2419 We have assumed a metallicity of $[\text{Fe}/\text{H}] = -2.12$ (Harris 1996) and a distance of 83.2 kpc (Ripepi et

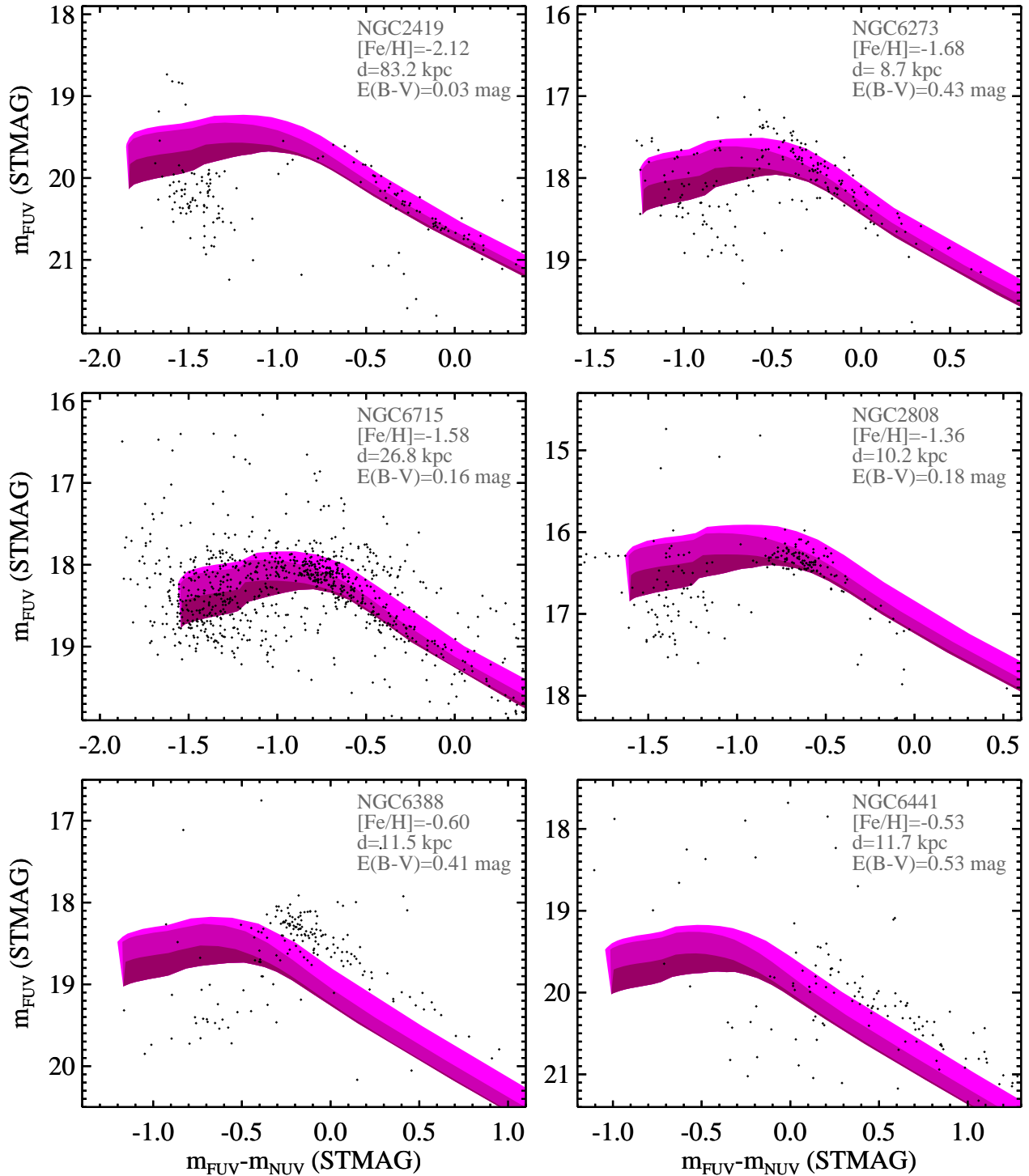


Figure 5. The ultraviolet CMDs shown in Figure 3, but restricted to the brighter and bluer stars in order to highlight the hot end of the HB. The canonical HB locus for each cluster is shown with shading to indicate evolutionary timescales; the three levels of shading, from darkest to lightest, indicate zero-age to 50% HB lifetime, 50% to 90% HB lifetime, and 90% to 99% HB lifetime.

al. 2007). For the reddening, our assumption of $E(B-V) = 0.03$ mag is somewhat lower than that assumed elsewhere (0.08–0.11 mag; Harris 1996; Piotto et al. 2002; Ripepi et al. 2007), but the upward shift in the models is required to align the observed and theoretical loci at the BHB. As one progresses blueward in $m_{FUV} - m_{NUV}$ color from 1.0 to -0.8 mag, the observed HB appears to slope slightly upward relative to canonical HB, but it is worth noting that optical CMDs spanning the B , V , and I bandpasses (Piotto et al. 2002; Ripepi et al. 2007) do not show a sloping HB that would justify normalizing the canonical locus significantly below the BHB. As one moves to stars bluer than the BHB, the observed HB locus drops abruptly to fainter magnitudes, such that nearly all of the observed EHB stars are subluminal (i.e., BH stars).

NGC 6273 We have assumed a metallicity of $[Fe/H] = -1.68$ and a distance of 8.7 kpc (Piotto et al. 2002). For the reddening, our assumption of $E(B-V) = 0.43$ mag is larger than that assumed by Piotto et al. (2002; 0.37 mag), shifting the theoretical locus fainter by ~ 0.5 mag in the far-UV to give alignment with the observed BHB. As with NGC 2419, the HB slope appears somewhat steeper than expected as one moves blueward from 0.5 mag to -0.5 mag in $m_{FUV} - m_{NUV}$ color, even though the optical CMD (e.g., Piotto et al. 2002) shows no indication of an upward HB slope from the red HB to the BHB. At the hot end of the HB, the observed population is roughly split between normal EHB stars and BH stars.

NGC 6715 We have assumed a metallicity of $[Fe/H] = -1.58$ and a distance of 26.8 kpc (Harris 1996). For the reddening, our assumption of $E(B-V) = 0.16$ mag is slightly higher than that assumed elsewhere (0.15 mag; Harris 1996; Siegel et al. 2007), shifting the models fainter by 0.08 mag to align with the observed BHB. The observed HB locus and the theoretical locus agree well over the entire BHB range, but at the EHB, the observed population is roughly split between normal EHB stars and BH stars. Note that NGC 6715 may actually represent the core of the disrupted Sgr dwarf galaxy (e.g., Layden & Sarajedini 2000; Siegel et al. 2007). Even if it is not the core of the Sgr dwarf, the earlier optical CMDs in this vicinity exhibit populations more complex than one would usually associate with a globular cluster, which may explain the large scatter in our UV CMD.

NGC 2808 This cluster was examined extensively in Paper I. The cluster is included here for comparison, and we assume the same cluster parameters used previously. Although the HB sample in NGC 2808 is smaller than that in NGC 6715, the morphology of the observed HB locus is similar. The similarities between the NGC 6715 and NGC 2808 CMDs may be related to the similarities in metallicity and central concentration; NGC 6273 is also close in metallicity, but is less centrally concentrated and less luminous than NGC 6715 and NGC 2808 (Harris 1996).

NGC 6388 We have assumed a metallicity of $[Fe/H] = -0.6$ and a distance of 11.5 kpc (Piotto et al. 2002). For the reddening, our assumption of $E(B-V) = 0.41$ mag is slightly larger than that of Piotto et al. (2002; 0.4 mag), placing the canonical locus 0.5 mag fainter than the observed BHB, as found by Busso et al. (2007) and discussed above. However, Busso et al. (2007) assumed a distance of 11.2 kpc and $E(B-V) = 0.45$ mag; if we adopted these values, the canonical HB locus would be an additional 0.3 mag fainter than we have assumed. In contrast, assuming the shorter distance (10 kpc) and lower reddening (0.37 mag) of Harris (1996) would align the canonical locus with the observed HB locus at the BHB, as we did for the metal-poor clusters. Although we have chosen

an extinction that places the canonical BHB 0.5 mag below the observed BHB, nearly all of the observed EHB stars are subluminal with respect to the theoretical locus, as also seen in NGC 2419. However, unlike the situation in NGC 2419, the subluminal EHB stars of NGC 6388 cover a much wider range of color than that seen in any of the metal-poor clusters; the subluminal EHB stars in NGC 2419 are well-separated in color from the BHB stars, but there is no such color gap in the NGC 6388 population. Despite their extension to unusually red colors, the subluminal EHB stars in NGC 6388 are much bluer than the BSS (see Figure 3), and thus there is no confusion between these two classes of stars. Moreover, the subluminal EHB stars in NGC 6388 comprise a contiguous and distinct group, which suggests that they may all be BH stars, including the reddest stars in this group.

NGC 6441 We have assumed a metallicity of $[Fe/H] = -0.53$, and a distance of 11.7 kpc (Harris 1996). For the reddening, our assumption of $E(B-V) = 0.53$ mag is larger than that of Harris (1996; 0.47 mag), placing the canonical locus 0.5 mag fainter than the observed BHB, as found by Busso et al. (2007) and discussed above. However, assuming the distance (15.2 kpc) and reddening (0.48 mag) of Busso et al. (2007) would place the canonical locus an additional 0.2 mag fainter than we have assumed. As with NGC 6388, assuming the Harris (1996) distance and reddening would align the canonical locus with the observed HB locus on the BHB, which is the normalization we used with the metal-poor clusters. Piotto et al. (2002) assumed a shorter distance (11.3 kpc) and less reddening (0.44 mag); assuming these values would place our models above the observed HB locus for all temperatures (i.e., not simply the potential BH stars). Regardless of the normalization, the colors imply that there are almost no stars hotter than $\sim 15,000$ K in the cluster on or below the canonical EHB. There are stars below the canonical HB in the temperature range of 10,000 – 15,000 K, which is hotter than the BSS. When considered in the context of the NGC 6388 BH population (which extends far to the red), it is possible that these subluminal stars in NGC 6441 are BH stars, despite their relatively red color. We inspected archival WFPC2 images in the F336W (U) and F439W (B) bands to determine where these unusually red BH candidates would fall in optical CMDs. Although the core of the cluster is crowded at these longer wavelengths, five such stars were sufficiently isolated to obtain clean photometry, and in the B vs. $U-B$ CMD they clearly fall within the low-luminosity end of the long blue HB tail, reinforcing the need for UV photometry to distinguish between temperature and luminosity variations in hot stars.

In all six clusters, the hottest HB stars observed are subluminal with respect to canonical models (see Figures 3 and 5). Thus there are BH stars in each cluster, with the possible exception of NGC 6441, where these subluminal stars are all relatively red. It is clear that canonical models at $Y = 0.23$ cannot explain the HB populations of these clusters. Regardless of how such models are normalized via varying the assumed reddening or distance, they cannot reproduce the observed luminosity difference between the BHB and the subluminal EHB stars.

4.2. Canonical Models with Enhanced Helium Abundance

We next consider models with the cluster metallicity but with the helium abundance increased to $Y = 0.4$. This value of helium enhancement is at the upper end of the plausible range for stars that have been enhanced at birth due to cluster self-enrichment. In Figure 6 we compare these models with

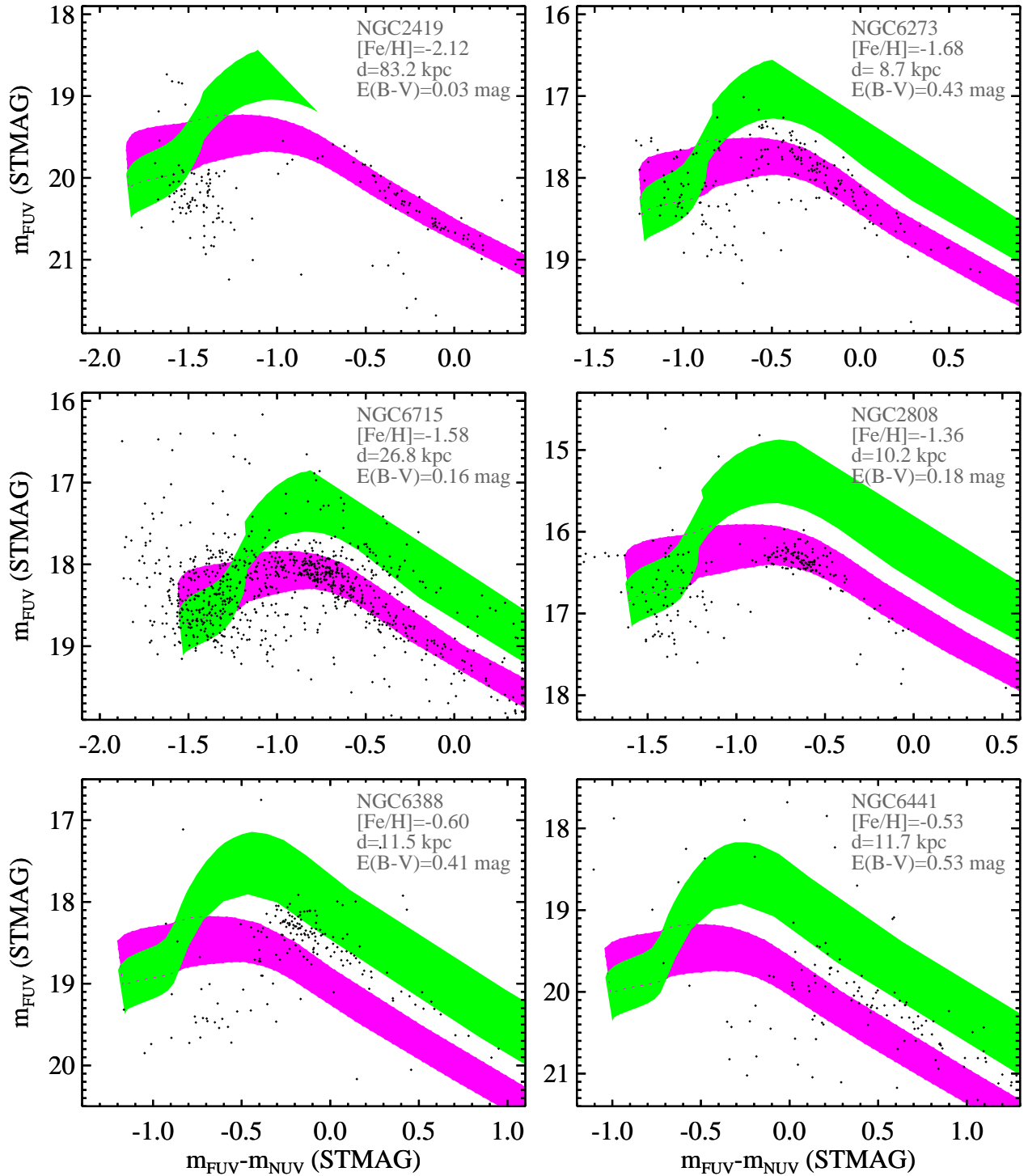


Figure 6. The same as in Figure 5, but with the canonical locus at standard helium abundance ($Y = 0.23$; violet) compared to the canonical locus with enhanced helium ($Y = 0.4$; green). The boundaries of the partly-observed $Y = 0.23$ locus are indicated for clarity (violet dashed lines).

$Y = 0.4$ to those with $Y = 0.23$, assuming the same cluster parameters ([Fe/H], distance, and reddening) used previously.

Figure 6 shows that an enhanced helium abundance produces a more pronounced dropoff in luminosity between the BHB and the EHB. Relative to the $Y = 0.23$ locus, the $Y = 0.4$ locus is fainter on the EHB but much brighter on the BHB. The fainter EHB luminosity of the $Y = 0.4$ locus is due to a slightly smaller core mass while the brighter BHB luminosity is due to a greater energy output of the H-burning shell. This dependence of the luminosity difference between the BHB and EHB on the helium abundance is well established and was evident even in the early HB calculations of Sweigart & Gross (1976). We note in Figure 6 that the $Y = 0.4$ models for the very metal-poor cluster NGC 2419 are restricted to hot temperatures, even for those HB stars that lost no mass on the RGB. This is because the main sequence turnoff mass for a population at $Y = 0.4$, [Fe/H]=−2.12, and an age of 13 Gyr is only $0.614 M_{\odot}$; this low turnoff mass, combined with this metal-poor composition, will only produce blue HB stars, even with no mass loss.

It is clear that the $Y = 0.4$ models do not agree well with the observed photometry when we assume the same parameters ([Fe/H], distance, and reddening) used in the $Y = 0.23$ models. The hot end of the $Y = 0.4$ locus is not as faint nor as red as the observed BH stars, and the cooler part of the $Y = 0.4$ locus is much brighter than the observed BHB stars. While a combination of the $Y = 0.23$ and $Y = 0.4$ models would lead to a larger luminosity width for the EHB, the predicted range in luminosity would still not extend to the faint magnitudes reached by the BH stars. It is also clear that any range in Y along the BHB must be fairly small, given the narrow luminosity width of the BHB loci in Figure 6. Note that the larger scatter in NGC 6715 may be due to the complex populations associated with the Sgr dwarf galaxy (Layden & Sarajedini 2000; Siegel et al. 2007).

At first glance, one might think that the agreement between $Y = 0.4$ locus and the observed BHB and EHB stars could be improved by assuming a larger reddening or distance, because such adjustments to the cluster parameters would shift the models to fainter magnitudes. Indeed, if the $Y = 0.4$ locus were shifted until it fit the observed BHB, the lower edge of the EHB for these models would be in much better agreement with the observed lower edge of the BH stars. However, such adjustments to the reddening or distance would violate important observational constraints.

If we attempt to fit the BHB with the $Y = 0.4$ locus, we will have to confront the following observational difficulties. Optical CMDs of NGC 2419 (Sandquist & Hess 2008), NGC 6273 (Piotto et al. 1999), NGC 6715 (Layden & Sarajedini 2000), or NGC 2808 (Bedin et al. 2000) do not show a significant difference in the V -band luminosity of the red HB and BHB stars, implying that any difference in the helium abundance between these stars must be small. Thus the cluster parameters we derived in fitting the BHBs of these clusters to the canonical $Y = 0.23$ locus should also apply to the red HB stars. In the case of the two metal-rich clusters NGC 6388 and NGC 6441, it is well known that the HB slopes upward (Rich et al. 1997; Busso et al. 2007), with the V -band luminosity of the BHB being ~ 0.5 mag brighter than that of the red HB clump. The BHB stars in these clusters may thus have an intermediate helium abundance ($Y \sim 0.3$). However, as discussed above, we took this offset in the BHB luminosity into account when fitting the $Y = 0.23$ model to our UV CMDs. Thus our parameters for these two clusters should also apply

to their red HB clumps. If the BHB should be dominated by stars with $Y = 0.4$ and the red HB by stars with $Y = 0.23$, one would therefore predict a luminosity difference between the BHB and red HB clump that is much larger than observed in any of our six clusters. To avoid this contradiction, one might argue alternatively that the red HB stars are themselves helium-rich, but this would imply a much brighter red HB luminosity and hence a much younger (and untenable) cluster age from the observed luminosity difference between the red HB and the MSTO (e.g., see Martín-Franch et al. 2010). As one example, Catelan et al. (2006) have compared the CMDs of NGC 6388 and 47 Tuc and concluded that both of these clusters have similarly old ages.

In short, while the $Y = 0.4$ locus exhibits a sharp drop in luminosity between the BHB and EHB, these models cannot by themselves explain the BH phenomenon. Given the lack of helium enhancement on the red HB and the relative luminosities of the BHB and red HB, we cannot align models of arbitrarily high Y to the BHB without violating other observational constraints. If we assume the BHB has a standard helium abundance ($Y = 0.23$, in the case of the four metal-poor clusters) or an intermediate helium abundance ($Y \sim 0.3$, in the case of the two metal-rich clusters), then even a wide range of helium abundance ($0.23 \lesssim Y \lesssim 0.4$) on the EHB would not explain either the faint luminosities or the wide color range observed in the BH stars.

4.3. Flash Mixed Models

We next consider models which undergo flash mixing due to high mass loss on the RGB. In Figure 7, we plot these flash-mixed models in our UV CMDs, assuming the same reddening and distance values obtained in section 4.1. Those values align a canonical $Y = 0.23$ locus to the BHB in the four metal-poor clusters, but place this $Y = 0.23$ locus 0.5 mag fainter (in m_{FUV}) than the BHB in the two metal-rich clusters. For each cluster in Figure 7 we show the HB evolutionary tracks for three representative flash-mixed models; two of these tracks fall at the extremes of the range in the mass loss rate leading to flash mixing, as measured by the value of η_R , while one falls halfway between these extremes. We plot these triplets of flash-mixed tracks for both $Y = 0.23$ and $Y = 0.4$ in order to bracket the range of behavior expected from any subpopulation in the cluster that undergoes enough mass loss for flash mixing. All of the flash-mixed tracks for each cluster fall within a narrow temperature range. The offset in luminosity among these tracks is due to small differences in the helium-core mass.

As can be seen in Figure 7, flash-mixed models can reproduce the faint luminosities observed in the BH population, particularly the flash-mixed models originating in a subpopulation with enhanced helium. Flash mixing thus offers a way of reproducing the faint luminosities observed in the BH stars without causing problems at the BHB or red HB clump, as discussed in the last section. Furthermore, the flash-mixed models, when combined with the canonical HB locus, are better able to reproduce the large luminosity width observed at the hot end of the EHB.

There is one obvious problem, however, which was also seen in the previous sections; like canonical models, flash-mixed models (whether originating in a population with enhanced or standard Y) cannot reproduce the red colors in the BH population. Paper I explored various ways of producing such red BH stars, including enhanced line blanketing in the

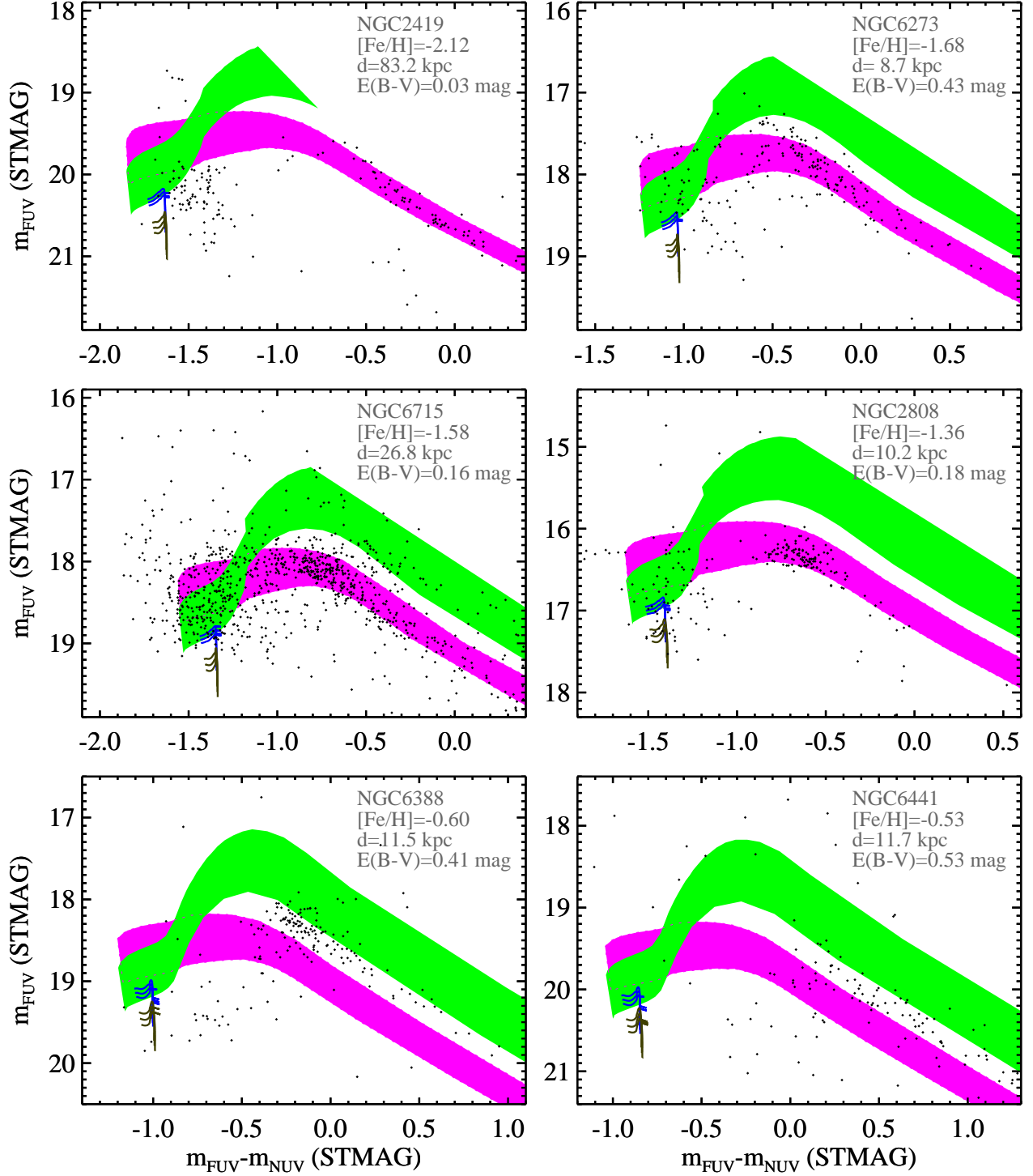


Figure 7. Our UV CMDs compared to canonical models at standard helium abundance ($Y = 0.23$; violet), canonical models at enhanced helium abundance ($Y = 0.4$; green), and flash-mixed models for stars born at standard helium abundance (blue curves) and enhanced helium abundance (brown curves). The combination of canonical and flash-mixed models is able to reproduce the full luminosity width of the observed EHB, but not the red colors seen in some of the BH stars.

atmosphere, due to an increase in the atmospheric Fe abundance via radiative diffusion. In the case of NGC 2808, an increase in the $[\text{Fe}/\text{H}]$ from -1.36 to $+1.0$ could shift the BH stars ~ 0.3 mag to the red. However, this color shift is not enough to explain the full color range of the BH population. Furthermore, the effect would be even smaller for the metal-rich clusters, which are the very clusters exhibiting the reddest BH stars. Because the metal-rich clusters already incur significant line blanketing, increasing the $[\text{Fe}/\text{H}]$ via diffusion does not help much; for example, increasing the $[\text{Fe}/\text{H}]$ in NGC 6388 from -0.6 to $+1.4$ only shifts the BH color redward by 0.26 mag. Thus, at this time, the mechanism for producing subluminal HB stars with such red colors remains a puzzle, and it suggests that the formation mechanism for these stars is not yet fully understood.

5. DISCUSSION

5.1. Blue Hook Stars

In this paper, we have compared the UV CMDs of six massive globular clusters with the expectations from stellar evolution theory. We find that in each of these clusters, the hottest HB stars are subluminal with respect to canonical models, whether or not those models assume a standard helium abundance ($Y = 0.23$) or an enhanced helium abundance ($Y = 0.4$). The most straightforward interpretation is that all of these clusters host BH stars. However, in the two metal-rich clusters, the subluminal stars either extend to relatively red colors (NGC 6388) or are restricted to these red colors (NGC 6441), which might imply that an additional or distinct phenomenon is at work at high metallicity. Indeed, the existence of BH stars in NGC 6441 has been questioned (e.g., Dieball et al. 2009). The BH population of NGC 6388 may be the link between the BH populations in the metal-poor clusters and that in NGC 6441, because it spans the full color range observed in these clusters. The bluest stars in the NGC 6388 BH population appear to be analogs of the BH stars in the metal-poor clusters, while the reddest stars in the NGC 6388 BH population appear to be analogs of the BH stars in the NGC 6441 population. Moreover, the entire BH population in NGC 6388 appears to be contiguous.

In some massive clusters, all of the EHB stars may have originated in a sub-population with enhanced helium. For example, in NGC 2808, nearly all of the EHB stars falling within the $Y = 0.23$ canonical locus (Figure 6; *pink shaded region*) also fall within the $Y = 0.4$ canonical locus (Figure 6; *green shaded region*); such stars are normal in the sense that they are not flash-mixed. However, there is a dearth of stars falling in the brighter part of the $Y = 0.23$ EHB locus, which may indicate that the dominant $Y = 0.23$ population in this cluster only produced BHB and red HB stars. In NGC 2419, the situation is even more extreme. Few EHB stars fall in either the $Y = 0.23$ or $Y = 0.4$ canonical loci, and thus all of the EHB stars in this cluster may have been produced via flash-mixing (see Figure 7). As with NGC 2808, the dominant $Y = 0.23$ population in NGC 2419 may only have produced BHB and red HB stars.

5.2. The Case for Flash Mixing

The faint luminosities observed in the BH stars can be reproduced by models that undergo flash mixing during a late helium-core flash on the WD cooling curve. Helium enhancements may also play an important role in the formation of BH stars, primarily because a higher helium abundance lowers the

MSTO mass at a given age so that less mass loss is required on the RGB to populate the hot HB. Helium enhancements also depress the luminosity somewhat in canonical EHB models, but not by the ~ 1 mag of the faintest BH stars.

Several recent studies have argued against flash mixing as the origin of the BH stars. For example, Lee et al. (2005) attribute the BH stars to the evolution of a population with a high initial helium abundance ($Y = 0.4$). However, as we demonstrate in §4.2, an enhancement in Y cannot by itself explain the BH phenomenon. While an enhanced Y decreases the EHB luminosity and increases the BHB luminosity (thus providing a hook at the hot end of the HB), one cannot arbitrarily adjust the cluster reddening and distance to match the theoretical HB locus to an observed CMD without regard to the relation between the BHB, the red HB, and the MSTO. Furthermore, the models of Lee et al. (2005) do not predict any carbon enhancement in the BH stars, while optical spectra of BH stars in ω Cen and NGC 2808 do suggest such an enhancement may be present (Moehler et al. 2004, 2007) – an enhancement naturally produced by flash-mixing.

D’Antona et al. (2010) go further, postulating that MS stars born at $Y \approx 0.4$ could undergo deep mixing on the RGB that elevates their helium abundance to $Y \approx 0.8$ before arrival on the EHB. The mechanism that drives this deep mixing is unclear, unlike the mechanism for flash mixing that follows from the basic stellar structure equations and which is the inevitable outcome of a helium-core flash on the WD cooling curve. However, the effect of the D’Antona et al. (2010) “RGB mixing” is to generate EHB stars with very high helium abundances that are hotter than the canonical HB, and in this way their models are similar to those produced by flash mixing. An important distinction, however, is that their RGB mixing precedes the helium-core flash, and thus does not produce an enhancement in the carbon abundance.

Castellani et al. (2006) have argued that canonical HB models can reach the high T_{eff} observed for BH stars, but their EHB stars reach a maximum T_{eff} of $\sim 32,000$ K. This is much less than that found by Moehler et al. (2004, 2007) for the BH stars ($> 35,000$ K), and much less than the temperatures reached by either flash mixing or RGB mixing models. Furthermore, canonical HB models would not produce any enhancements in helium or carbon, as observed for such stars (Moehler et al. 2004, 2007).

In Paper II, we found that a delayed helium-core flash could sometimes lead to a more shallow form of flash mixing, where the envelope hydrogen is only mixed into the outer layers of the core. When this happens, flash-mixed stars can retain some residual envelope hydrogen, and consequently would be distributed closer to the canonical EHB. Our models imply that shallow mixing may be a relatively rare occurrence, especially at low metallicities. Our CMDs do not show any systematic variation in the number of BH stars falling close to the canonical locus, suggesting that shallow mixing is not important in the metallicity range covered by our clusters. It may be, however, that we simply do not have enough BH stars to detect such a trend. With the current sample, it appears that the BH stars in each cluster fall up to ~ 1 mag below the canonical HB, regardless of metallicity.

The sdB and sdO stars of the Galactic field are the analogs of the EHB and post-EHB stars found in clusters. One would expect some of these stars to also show evidence of flash mixing. This expectation motivated far-UV spectroscopy of helium-rich sdB stars in the Galactic field using the *Far Ultraviolet Spectroscopic Explorer*, to see if these stars exhibit the

helium and carbon abundance enhancements expected from flash mixing. Those observations do in fact lend support to the flash mixing scenario. The spectrum of PG1544+488 (archetype of the He-sdB class) shows incredibly strong carbon lines, indicating a surface that is $\approx 2\%$ carbon by mass (Paper II).

Further insight into the nature of the BH stars may come from upcoming far-UV spectroscopy of NGC 2808. In the current observing cycle, we will use the Space Telescope Imaging Spectrograph on *HST* to obtain spectra of BH stars, normal EHB stars, and BHB stars selected from the NGC 2808 CMD (Figure 5). With these spectra, we will be able to search for the atmospheric signatures of flash mixing (e.g., enhanced carbon, diminished H) and perhaps shed light on the origin of the wide color range exhibited in BH stars.

Our understanding of the BH phenomenon is far from complete. None of the models discussed in this paper (canonical at standard Y , canonical at enhanced Y , or flash-mixed) are able to explain the red colors found in some or all of the subluminal stars in each cluster. This is particularly true in the two metal-rich clusters in our sample. Furthermore, the near-total lack of normal EHB stars in half of our clusters is puzzling. If we consider the categories of HB stars (red HB, BHB, normal EHB, BH) as a sequence governed by cluster parameters (mass loss, helium abundance, cluster mass, etc.), why do some clusters (NGC 2419, NGC 6388, and NGC 6441) exhibit BHB stars and BH stars but few normal EHB stars? The dearth of such stars may imply a gap in one or more cluster parameters, but the mechanism for such a gap is unclear.

5.3. Why Massive Clusters?

A remarkable feature of all clusters either known or suspected to host BH stars is that they are among the most massive clusters in the Galaxy. Dieball et al. (2009) also noted that BH stars only appear to exist in massive clusters, and suggested that this could simply be a statistical effect, because “intrinsically rare objects can only be found by searching a sufficiently large number of stars.” To examine this possibility, Dieball et al. (2009) apply a statistical test by comparing the locations of clusters with and without significant BH populations within the cumulative mass distribution of the clusters in their sample. Although Dieball et al. (2009) state that their analysis is “effectively combining many low-mass clusters to form aggregate high-mass clusters,” their test, in fact, ignores the actual numbers of BH stars in each cluster, and instead only considers whether clusters do or do not host significant numbers of BH stars. This is a difficult test, given the small number of clusters in their comparison. Although Dieball et al. (2009) suggested that it would be worthwhile to investigate how the numbers of BH stars scale with cluster properties, they did not actually perform this test due to the non-uniformities in the extant data. A uniform data sample would be important if one were trying to address the total size of the BH population as a function of cluster mass. However, the Dieball et al. (2009) sample already contains sufficient data to explore the relationship between BH population size and cluster mass. If the UV imaging is sufficient to produce a statistically significant sample of EHB stars in each cluster, one can ask if a significant fraction of the EHB stars are BH stars, and can then compare this fraction in clusters of different masses. This comparison is meaningful even if different clusters are observed in distinct ways (e.g., differences in region sampled, bandpasses used, depth); the important point is to observe a large enough sample of EHB stars to determine

the relative numbers of normal and subluminal (BH) EHB stars.

We refer to Table 2 of Dieball et al. (2009). Their table lists 5 clusters hosting significant numbers of BH stars (NGC 2419, NGC 2808, ω Cen, NGC 6388, and NGC 6715). All of these clusters have masses ranging from $1.42 \times 10^6 M_{\odot}$ (NGC 2808) to $3.35 \times 10^6 M_{\odot}$ (ω Cen). We would add NGC 6273 to this list; because it is 0.2 mag fainter in M_V than NGC 2808 (Harris 1996), its mass is $\approx 1.2 \times 10^6 M_{\odot}$. Table 2 of Dieball et al. (2009) also lists 11 clusters that do not have significant numbers of BH stars. Of course, besides these 11 clusters, there are many more low-mass and intermediate-mass clusters without known BH stars, but these 11 were considered by Dieball et al. (2009) to have sufficient imagery to rule one way or the other. Among that list of 11 clusters is NGC 6441, with a mass of $1.57 \times 10^6 M_{\odot}$; we would move it to the list of clusters hosting BH stars. Also in that list of 11 clusters is NGC 104 (47 Tuc); it is massive ($1.5 \times 10^6 M_{\odot}$), but it is the only cluster in the entire table that has no BHB stars (its HB population is entirely red). The total mass of the 9 remaining clusters in this list is $5.1 \times 10^6 M_{\odot}$. The stellar mass in this ensemble of 9 clusters exceeds the mass in any individual cluster, and is twice the mass of any cluster we have explored in our own study. Although this ensemble is comprised of 9 clusters hosting BHB stars and in some cases (e.g., M13, M80, NGC 6752) substantial populations of EHB stars, this ensemble has few if any BH stars (possibly 3–5; Dieball et al. 2009; Sandquist et al. 2010). If finding BH stars simply required the searching of enough stellar mass, we would expect to find tens of BH stars in the ensemble mass of 9 clusters totaling $5.1 \times 10^6 M_{\odot}$. The implication is that any cluster hosting BHB stars will also host BH stars if its mass exceeds $\sim 1.2 \times 10^6 M_{\odot}$. However, the fraction of EHB stars that are subluminal varies from cluster to cluster in our sample, and that fraction does not appear to correlate with either cluster mass or metallicity, implying additional factors are at work (including perhaps the dynamical history of interactions between the cluster and the Galaxy). In half of our sample (NGC 2419, NGC 6388, and possibly NGC 6441), virtually all of the EHB stars appear to be BH stars, with very few stars on the canonical EHB, whereas in the remaining three clusters (NGC 6273, NGC 6715, and NGC 2808), the split between normal and subluminal EHB stars appears to be roughly equal.

Note that low-mass clusters can have large samples of EHB stars without having any BH stars. Consider NGC 6752, which is one of the 9 clusters discussed above that hosts no BH stars; it is listed in Table 2 of Dieball et al. (2009) with a mass of $0.32 \times 10^6 M_{\odot}$. For NGC 6752 (Landsman et al. 1996) and NGC 2808 (Paper I), there exist CMDs that include a far-UV bandpass. In the case of NGC 6752, the CMD is sampling a less massive cluster outside of the core, while in the case of NGC 2808, the CMD is sampling a more massive cluster within the core. Despite these distinctions, the samples of EHB stars and their descendants are comparable in size. In each CMD, there are ~ 80 HB stars hotter than 16000 K, along with four post-EHB stars – i.e., the shorter-lived AGBM stars. However, for the case of NGC 2808, 46 of the EHB stars are BH stars (lying well below the canonical EHB), while in NGC 6752, none of them are. Given that the size of the EHB samples are approximately the same, the number of BH stars in the two clusters are discrepant at a high statistical significance. This argument is not restricted to NGC 6752; other

low-mass clusters, such as M13 and M80 (Ferraro et al. 1998) host dozens of EHB stars but apparently few if any BH stars (M13 may host 2 BH stars; Sandquist et al. 2010). The large numbers of EHB stars in both the low-mass cluster sample and the high-mass cluster sample provide strong support for the notion that the fraction of EHB stars that are subluminoous (i.e., BH stars) is nearly zero in low-mass clusters and $\sim 50\text{--}100\%$ in high-mass clusters.

There are several possible reasons why BH stars may only appear in massive globular clusters. One possibility is that only massive clusters can retain the helium-rich ejecta from their first generation of stars. Besides this helium enrichment, such self-pollution might account for many of the abundance variations in O, Na, Mg and Al observed in MS and RGB stars (see Gratton et al. 2004 and references therein).

An alternative hypothesis is that massive clusters have many close binaries, which produce the high mass loss needed for flash mixing. Of the massive clusters known to host BH stars, none are core-collapsed, and all are of intermediate central concentration (Harris 1996), so that one might expect a significant fraction of surviving binaries (Ivanova et al. 2005). However, the lack of a radial gradient in the NGC 2808 BH population argues against a binary origin (Bedin et al. 2000).

Support for proposal 10815 is provided by NASA through a grant from STScI, which is operated by AURA, Inc., under NASA contract NAS 5-26555. We thank the anonymous referee for comments that helped improve the clarity of this paper.

REFERENCES

- Anderson, J. 1997, Ph.D. thesis, UCB
- Anderson, J., Piotto, G., King, I.R., Bedin, L.R., & Guhathakurta, P. 2009, *ApJ*, 697, L58
- Bedin, L.R., Piotto, G., Anderson, J., Cassisi, S., King, I.R., Momany, Y., & Carraro, G. 2004, *ApJ*, 605, L125
- Bedin, L.R., Piotto, G., Zoccali, M., Stetson, P.B., Saviane, I., Cassisi, S., & Bono, G. 2000, *A&A*, 363, 159
- Bekki, K., & Norris, J.E. 2006, *ApJ*, 637, L109
- Brown, T.M., Bowers, C.W., Kimble, R.A., Sweigart, A.V., & Ferguson, H.C. 2000, *ApJ*, 532, 308
- Brown, T.M., Ferguson, H.C., Davidsen, A.F. & Dorman, B. 1997, *ApJ*, 482, 685
- Brown, T.M., Smith, E., Ferguson, H.C., Sweigart, A.V., Kimble, R.A., & Bowers, C.W. 2008, *ApJ*, 682, 319
- Brown, T.M., Sweigart, A.V., Lanz, T., Landsman, W.B., & Hubeny, I. 2001, *ApJ*, 562, 368 (Paper I)
- Busso, G., et al. 2007, *A&A*, 474, 105
- Carney, B.W. 1996, *PASP*, 108, 900
- Cassisi, S., Schlattl, H., Salaris, M., & Weiss, A. 2003, *ApJ*, 582, L43
- Castellani, M., & Castellani, V. 1993, *ApJ*, 407, 649
- Castellani, V., Iannicola, G., Bono, G., Zoccali, M., Cassisi, S., & Buonanno, R. 2006, *A&A*, 446, 569
- Castelli, F., & Kurucz, R.L. 2003, in *IAU Symposium 210, Modeling of Stellar Atmospheres*, eds. N. Piskunov, W.W. Weiss, & D.F. Gray, poster A20, astro-ph/0405087
- Catelan, M., Stetson, P.B., Pritzl, B.J., Smith, H.A., Kinemuchi, K., Layden, A.C., Sweigart, A.V., & Rich, R.M. 2006, *ApJ*, 651, L133
- Chiaberge, M., Pey Lian, L., Kozhurina-Platais, V., Sirianni, M., & Mack, J. 2009, *Instrument Science Report ACS 2009-01*
- Cunha, K., Hubeny, I., & Lanz, T. 2006, *ApJ*, 647, L143
- D'Antona, F., Bellazzini, M., Caloi, V., Pecci, F.F., Galletti, S., & Rood, R.T. 2005, *ApJ*, 631, 868
- D'Antona, F., Caloi, V., Montalbán, J., Ventura, P., & Gratton, R. 2002, *A&A*, 395, 69
- D'Antona, F., Caloi, V., & Ventura, P., 2010, *MNRAS*, in press, astro-ph/1003.2052
- D'Cruz, N.L., Dorman, B., Rood, R.T., & O'Connell, R.W. 1996, *ApJ*, 466, 359
- D'Cruz, N.L., O'Connell, R.W., Rood, R.T., Whitney, J.H., Dorman, B., Landsman, W.B., Hill, R.S., Stecher, T.P., & Bohlin, R.C. 2000, *ApJ*, 530, 352
- Dieball, A., Knigge, C., Maccarone, T.J., Long, K.S., Hannikainen, D.C., Zurek, D., & Shara, M. 2009, *MNRAS*, 394, L56
- Dolphin, A.E. 2000, *PASP*, 112, 1397
- Ferraro, F.R., Paltrinieri, B., Fusi Pecci, F., Rood, R.T., & Dorman, B. 1998, *ApJ*, 500, 311
- Ferraro, F.R., Sollima, A., Pancino, E., Bellazzini, M., Straniero, O., Origlia, L., & Cool, A.M. 2004, *ApJ*, 603, L81
- Fitzpatrick, E.L. 1999, *PASP*, 111, 63
- Fruchter, A.S., & Hook, R.N. 2002, *PASP*, 114, 144
- Gratton, R., Sneden, C., & Caretta, E. 2004, *ARAA*, 42, 385
- Han, S.-I., Lee, Y.-W., Joo, S.-J., Sohn, S.T., Yoon, S.-J., Kim, H.-S., and Lee, J.-W. 2009, *ApJ*, 707, L190
- Harris, W.E. 1996⁸, *AJ*, 112, 1487
- Heyer, I., Richardson, M., Whitmore, B., Lubin, L. 2004, *WFPC2 Instrument Science Report WFPC2 2004-001*
- Hubeny, I., & Lanz, T. 1995, *ApJ*, 439, 875
- Ivanova, N., Belczynski, K., Fregeau, J.M., & Rasio, F.A. 2005, *MNRAS*, 358, 57 2
- Landsman, W.B., Sweigart, A.V., Bohlin, R.C., Neff, S.G., O'Connell, R.W., Roberts, M.S., Smith, A.M., & Stecher, T.P. 1996, *ApJ*, 472, L93
- Lanz, T., Brown, T.M., Sweigart, A.V., Hubeny, I., & Landsman, W.B. 2004, *ApJ*, 602, 342 (Paper II)
- Lanz, T., & Hubeny, I. 2003, *ApJS*, 146, 417
- Lanz, T., & Hubeny, I. 2007, *ApJS*, 169, 83
- Layden, A.C., & Sarajedini, A. 2000, *AJ*, 119, 1760
- Lee, Y.-W., Joo, S.-J., Han, A.-I., Chung, C., Ree, C.H., Sohn, Y.-J., Kim, Y.-C., Yoon, S.-J., Yi, S.K., & Demarque, P. 2005, *ApJ*, 621, L57
- Martín-Franch, A., Cassisi, S., Aparicio, A., & Pietrinferni, A. 2010, *ApJ*, in press, astro-ph/1003.5489
- Maybhatte, A., et al. 2010, "ACS Instrument Handbook," Version 9.0 (Baltimore: STScI).
- Miller Bertolami, M.M., Althaus, L.G., Unglaub, K., & Weiss, A. 2009, *JPhCS*, 172, 12014
- Milone, A.P., et al. 2008, *ApJ*, 673, 241
- Moehler, S., Dreizler, S., Lanz, T., Bono, G., Sweigart, A.V., Calamida, A., Monelli, M., & Nonino, M. 2007, *A&A*, 475, L5
- Moehler, S., Sweigart, A.V., Landsman, W.B., Hammer, N.J., & Dreizler, S. 2004, *A&A*, 415, 313
- Piotto, G., Bedin, L.R., Anderson, J., King, I.R., Cassisi, S., Milone, A.P., Villanova, S., Pietrinferni, A., & Renzini, A. 2007, *ApJ*, 661, L53
- Piotto, G., et al. 2002, *A&A*, 391, 945
- Piotto, G., et al. 2005, *ApJ*, 621, 777
- Piotto, G., Zoccali, M., King, I.R., Djorgovski, S.G., Sosin, C., Rich, R.M., & Meylan, G. 1999, *ApJ*, 118, 1727
- Reimers, D. 1975, *Mém. Roy. Soc. Liège*, 8, 369
- Reimers, D. 1977, *A&A*, 57, 395
- Renzini, A. 1990, in *ASP Conf. Ser. 11, Confrontation Between Stellar Pulsation and Evolution*, ed. C. Cacciari & G. Clementini (San Francisco: ASP), 549
- Renzini, A. 2008, *MNRAS*, 391, 354
- Rich, R.M., et al. 1997, *ApJ*, 474, L25
- Ripepi, V., et al. 2007, *ApJ*, 667, L61
- Rosenberg, A., Recio-Blanco, A., Garcá-Mari, M. 2004 *ApJ*, 603, 135
- Salaris, M., Chieffi, A., & Straniero, O. 1993, *ApJ*, 414, 580
- Sandquist, E.L., Gordon, M., Levine, D., & Bolte, M. 2010, *AJ*, 139, 2374
- Sandquist, E.L., & Hess, J.M. 2008, *AJ*, 136, 2259
- Sirianni, M., et al. 2005, *PASP*, 117, 1049
- Siegel, M.H., et al. 2007, *ApJ*, 667, L57
- Sweigart, A.V. 1997, in *The Third Conference on Faint Blue Stars*, ed. A.G.D. Phillip, J. Liebert, & R.A. Saffer (Schenectady: L. Davis Press), 3
- Sweigart, A.V., & Gross, P.G. 1976, *ApJS*, 32, 367

⁸ Updated at <http://physicswww.physics.mcmaster.ca/~harris/mwgc.dat>